# Numerical Simulation of the Chemical Combination and Dissociation Reactions of Neutral Particles in a Rarefied Plasma Arc Jet

Jie Li, Derek Ingham, Lin Ma, Ning Wang, and Mohamed Pourkashanian

**Abstract— The expansion of neutral particles in a plasma arc jet is crucial for the distribution of the ions and electrons, especially in an unsteady rarefied plasma arc jet with chemical reactions. A three-dimensional unsteady investigation of neutral particles in a rarefied flow with chemical combination and dissociation reactions is numerically simulated based on an in-house direct simulation Monte Carlo (DSMC) code. The evolution of the neutral particles flow in vacuum cylinders is presented, and the influence of the chemical reactions have been investigated for the neutral particles. The predicted results imply that the dissociation reaction plays a key role in the expansion of the neutral particles process. In order to study the expansion of the neutral particles in an electric field, an electrostatic particle-in-cell (PIC) and DSMC are combined to simulate the axisymmetric rarefied plasma flows with chemical reactions. Two sets of grids are employed for the DSMC/PIC method by considering the different requirements of both the methods based on the molecule mean free path and the Debye length. The properties of both the flow and electric fields are analyzed in detail. It is found that the electric potential increases if the initial velocity of the ions from the inlet is sufficiently large, and accordingly, the number density of the ions in the flow field increases further.**

**Index Terms—Direct simulation of Monte Carlo (DSMC), particle-in-cell (PIC), plasma arc jet.**

## I. Introduction

Plasma arc jets are widely employed in the fields of aerospace propulsion [1]-[3], industrial coatings [4], [5] and nuclear fusion reactors [6], [7], such as the plasma thruster in electric propulsion systems [2] and the developing of micro cathode arc thrusters [3] employed in the micro satellites. In these devices, where plasma arc jets flow, the dimensions are sometimes very small and this results in the flow field being not a continuum, and the particles in the jet are very dilute and interact with each other only occasionally [8]. The parameter that represents the degree of this rarefaction of the gas flow is the Knudsen number, and this is the ratio of the molecules' mean free path to the characteristic dimension of the flow. When the plasma jet is very rarefied and the Knudsen number is larger than about 0.1, the Navier-Stokes equations become unsuitable. Therefore a kinetic theory approach, such as the direct simulation Monte Carlo (DSMC) method, should be employed for these flows [9]. In the rarefied plasma transport processes, neutral particle diffusion have an impact on the movement of the ions and electrons, especially in the rarefied plasma flow of a cathodic vacuum arc [10], [11], where neutral particle collisions as well as chemical dissociation and recombination reactions have an important role in the distribution of the charged particles during the diffusion process. The main numerical simulation DSMC/PIC method is currently used to solve such plasma transport problems in a rarefied environment [2], [3], [6]-[8], [10]-[12]. The PIC method can simulate the movement of charged particles in a self-consistent electrostatic field, and the DSMC method can be implemented to simulate the particle movement and collisions between neutral particles as well as charged particles. The DSMC/PIC method combines the advantages of the DSMC and PIC methods, and this method can be used to describe some other complex physical phenomena in the plasma arc jet flow. Timko et al. [10] have investigated the one-dimensional plasma build-up in vacuum arcs by employing the PIC method, and it is shown that the evaporation of the neutral particles from the field emitter tip is the key factor in the arc development under vacuum conditions. Moore et al. [13] have employed the DSMC/PIC method to study the breakdown in various microscale electrode gaps under an atmospheric pressure. Both of the above mentioned studies were based on one-dimensional simulations, however, these works are a good starting point for the study of rarefied plasma vacuum arc flows.

Recently, Tsuno et al. [14] have studied supersonic rarefied weakly ionized plasma flows for the expanding arc jet in a diverging magnetic field, and the ions and the neutrals were treated by the particle scheme in the DSMC method, while the electrons are treated by the fluid scheme with a self-consistent electric field. Korkut et al. [2] have developed an adaptive mesh refinement combined with the Octree method for the

Manuscript received April, 2016. This work was supported in part by the National Natural Science Foundation of China under Grant 11272350.

Jie Li is both with College of Aerospace Science and Engineering, National University of Defense Technology, Changsha, 410073, China (e-mail: lijie_gfkd@163.com) and with Department of Mechanical Engineering, University of Sheffield, S10 2TN, UK (e-mail: jie.li@sheffield.ac.uk)

Derek Ingham, Lin Ma, and Mohamed Pourkashanian are with Energy-2050, Department of Mechanical Engineering, University of Sheffield, S10 2TN, UK (e-mail: d.ingham@sheffield.ac.uk; lin.ma@sheffield.ac.uk; m.pourkashanian@sheffield.ac.uk)

Ning Wang was with College of Aerospace Science and Engineering, National University of Defense Technology, Changsha, 410073, China (e-mail: wangning_nudt@163.com)

DSMC/PIC to study the 3-D plasma plume flow of small ion thrusters. The above studies have shown that the neutral particle diffusion in the rarefied plasma flow cannot be ignored, and from which the current study is mainly focused on the steady flow, while a study on the unsteady plasma arc jet flow with chemical reaction needs to be developed, and the understanding of the mechanism of neutral particles in this unsteady plasma arc jet flow is essential. Thus, in this paper, the in-house DSMC program has been employed to simulate the 3-D unsteady neutral particle expansion in a rarefied plasma arc jet with chemical combination and dissociation reactions, and it has been combined with the PIC method to simulate the plasma symmetric flow field and the electric field. The distribution of electronic potential and particle number density are obtained by performing statistical calculations, and the results obtained can provide the basic data for the further study of unsteady plasma arc jet flows with chemical reactions.

## II. VALIDATION OF THE IN-HOUSE DSMC PROGRAM

Due to the rarefied plasma arc jet flow conditions, the continuum CFD based approaches become unsuitable, and therefore a kinetic theory approach, such as the DSMC method must be used for these flows. The DSMC method is a physically based probabilistic simulation, and it is widely used to solve such problems. We have developed an in-house DSMC program and it has been used to simulate this flow. In order to verify its accuracy, we have employed this program to simulate a molecular hydrogen beam flow derived from [15], and these results have been compared with our results. The numerical domain and grids employed are shown in Fig.1. The boundary conditions are represented by the different colours, namely the red coloured parts represent the inlet boundary, the brown and black ones represent the wall boundary and the green ones are the free flow boundary. The molecular hydrogen beam from the entrance first enters into a converged tube as shown in zone 1 of Fig.1. The walls labelled “a” and “b” divide the flow field into three zones such as zone 2, zone 3 and zone 4 as shown in Fig. 1. The flow field is axisymmetrical, and the calculation conditions are listed as follows: the velocity of the molecular hydrogen that is introduced into the flow field is $V_x$=75 m/s, $V_y$=0, $V_z$=0, the number density is $10^{22}$ /m$^3$ and the temperature is 300 K. The temperature of the brown coloured wall is 100 K while for the black colored wall it is 300 K. In the simulation, 18684 nodes and 83496 tetrahedral volume elements are used for sampling and collision calculations. The time step is about $10^{-8}$ s, and the solutions were averaged over 10000 iterations. The number density contour of the molecular hydrogen beam is displayed in Fig. 2. The results for comparison of the number density, the temperature and the velocity are shown in Fig. 3 - Fig. 7 in which the black dots are the result of [15] and the red line is the result obtained by employing the in-house DSMC code. The comparison between these two sets of results show that there is no obvious discrepancy, and therefore the in-house DSMC program can be employed here.

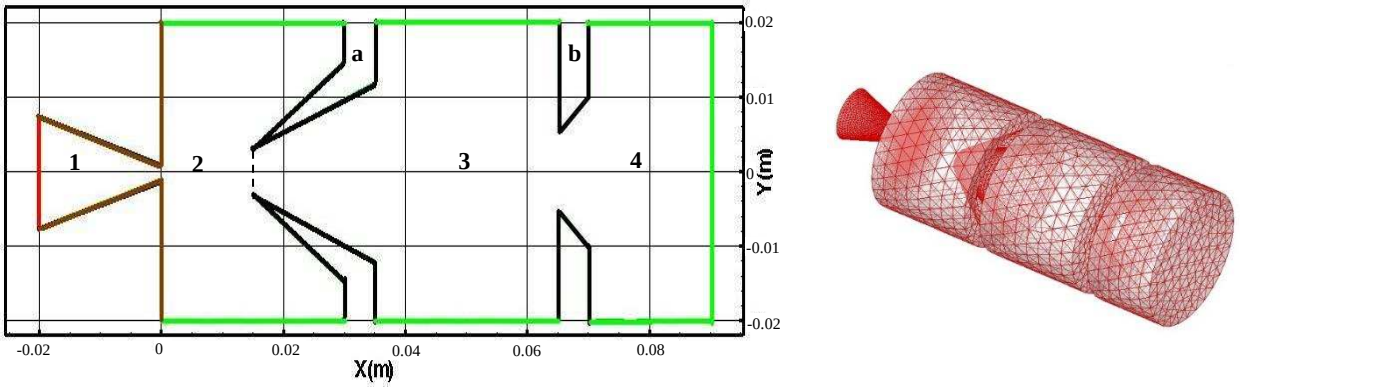


Fig. 1. The geometry and grids employed in the simulations. The axisymmetric geometry is obtained from [15], and the grids used in the in-house DSMC program are unstructured.

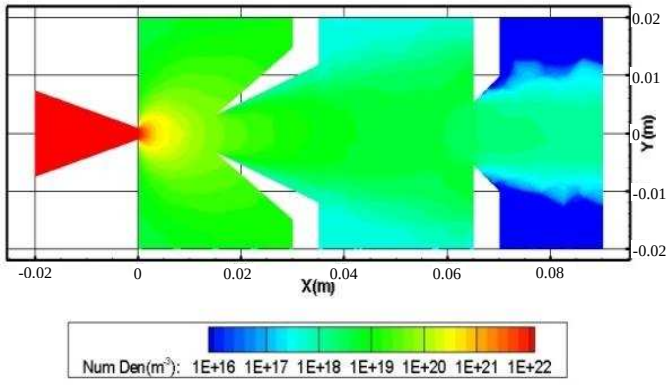


Fig. 2. Number density distribution of a molecular hydrogen $H_2$ beam.

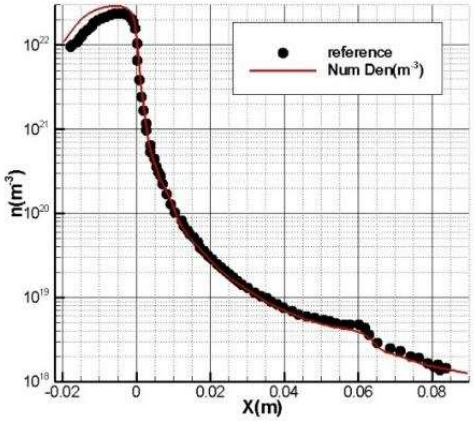


Fig. 3. Comparison of the on-axis number density. The results from [15] are represented by the black dots, and the red line represents the result obtained when employing the in-house DSMC code.

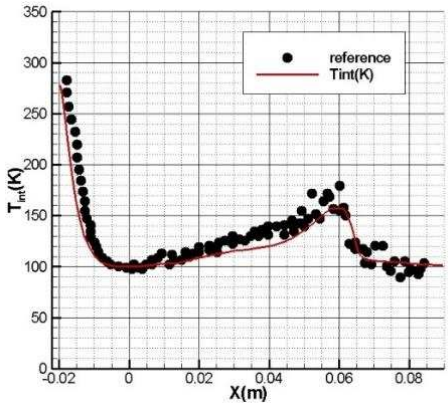


Fig. 4. The on-axis rotational temperature as a function of the axial distance.

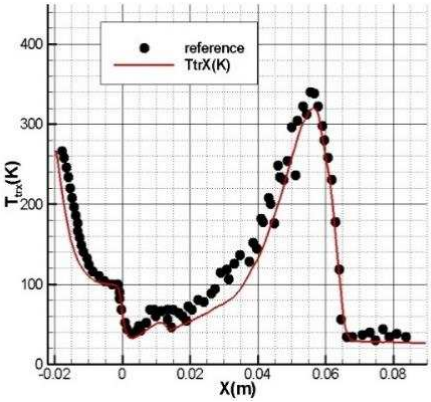


Fig. 5. The on-axis translational temperature in the X direction as a function of the axial distance.

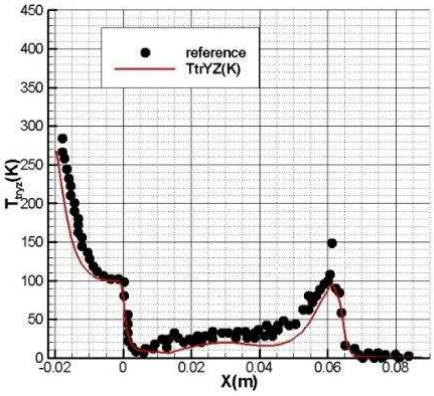


Fig. 6. The on-axis translational temperature in the YZ direction as a function of the axial distance.

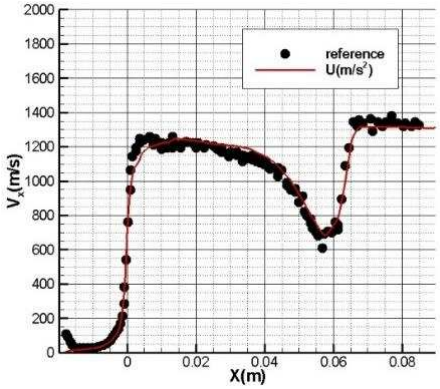


Fig. 7. The on-axis particle mean velocity in the X direction as a function of the axial distance.

## III. Numerical simulation of the 3-D unsteady neutral particles chemically reactive rarefied flow

### A. Simulation conditions

The calculation domain consists of two cylinders with different diameters, namely 5 mm and 15 mm. For each of them, the cylindrical height is the same as the diameter. There is a cylindrical jet exit with diameter 100 μm on the side of the small cylinder, and the particles are expanding into these two vacuum cylinders from the jet exit. These particles are composed of molecular hydrogen $H_2$ and atom hydrogen H, as are the other neutral species labelled X. During the unsteady emission process of the particles, the chemical reactions occur simultaneously. Here the recombination and dissociation reactions of the hydrogen are considered, and the chemical reaction equations are as follows:

$$H_2 + X \rightarrow 2H + X \tag{1}$$

$$2H + X \rightarrow H_2 + X \tag{2}$$

The number density of the particles from the jet exit is variable, and it is a function of the time as follows:

$$f = \begin{cases} 5\times10^{24}\sin\left(\pi - 5.46\times10^{5}\left(5\times10^{-6} - t\right)\right), & 0 \le t \le 5\mu s; \\ 0, & 5\mu s \le t. \end{cases} \tag{3}$$

The molar proportions of $H_2$, H and X are 0.3:0.3:0.4, the temperature of the particles is 3000 K and the velocity of the particles is 50000 m/s. The bottom of the larger cylinder is open to the vacuum, and the wall temperature for each cylinder is 300 K. The variable hard sphere (VHS) model [9] is used for the binary molecular collisions, and the diffusion reflection model [9] is used for the gas-surface interaction.

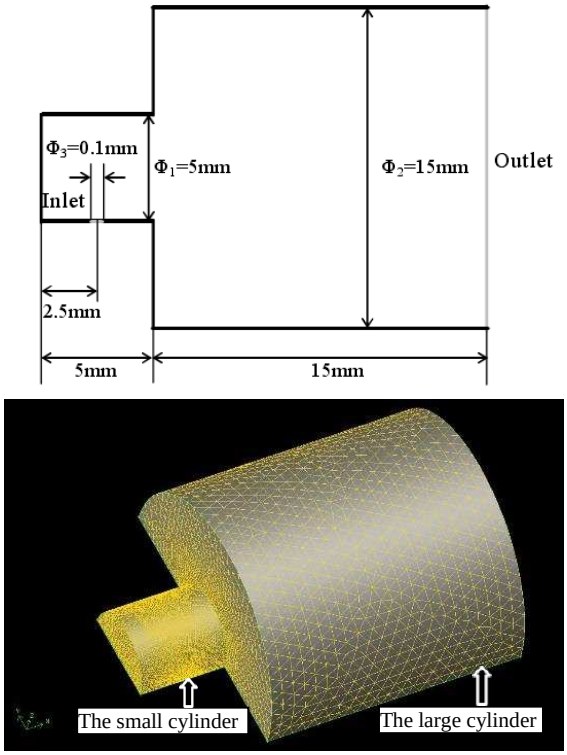


Fig. 8. The geometry and grids employed in the simulations. The geometry consists of two cylinders, the larger cylinder is open to the vacuum, and there is an inlet on the side wall of the smaller cylinder. The grids are unstructured.

TABLE I
PROPERTIES FOR THE VHS MOLECULAR MODEL AT 273K

| Gas | Diameter ($\times 10^{-10}$ m) | Molecular mass ($\times 10^{-27}$ kg) | Viscosity index |
|---|---|---|---|
| $H_2$ | 2.92 | 3.34 | 0.67 |
| H | 2.748 | 1.67 | 0.8353 |

B. Results and discussion

In the numerical simulation, 18799 nodes and 91962 tetrahedral volume elements are used. The time step is about $4\times10^{-10}$ s, and the computations were stopped after about 20000 iterations. Fig. 9 shows the total particle number density contour in the symmetrical plane without (upper) and with (lower) the chemical reactions, and this shows that the distribution of the total particle number density varies with time, basically the procedures of the evolution are the same, no matter whether the chemical reactions are considered or not. The particles flow from the jet exit in the bottom side wall of the smaller cylinder, then collide with the upper side wall and keep moving. When the collisions with the wall occur, the diffusion reflections make the reflected particles disperse isotropically. However, some reflected particles collide with the incident particles, and the number density of the incident particles are large and hinder the movement of these reflected particles. It can be clearly seen from Fig. 9 that the main jet stream density is high, and the angle between the incident particle stream and the reflected particle stream can be easily observed. The particles located in the left hand region continue to collide with the bottom and the side walls of the smaller cylinder, and then move to fill in the entire region of the smaller cylinder. For the particles located on the right hand region, some of them collide with the side wall of the smaller cylinder, whilst the others move directly into the larger cylinder. Some of these particles that are moving into the larger cylinder collide with the lower side wall of the cylinder, thus in the region near the larger cylinder, the particles first move near to the bottom side wall, then move towards the upper side wall. After the jet stops injecting the particles, the distribution of the particles in the flow field begins to become homogeneous. Fig. 9 shows a comparison of the results obtained both with and without the chemical reaction models, and the particle expansion process becomes faster when the chemical reactions are considered. When the flow period is 2 μs, the particles have already moved to the upper region of the larger cylinder. As the flow develops, the particle number density in this region is larger than that without the chemical reactions. At the time 6 μs, most of the particles have spread into the central region of the large cylinder, thus when considering the chemical reactions, the distribution of the particles has become almost constant. However, after the particles stop being injected, the opposite phenomenon can be observed. This is as shown at the time 8 μs, where the particle number density in the central region of the larger cylinder is significantly less than that in the region near the wall. The dissociation reaction is mainly attributed to this phenomenon. In the flow field, the combination reaction for atomic hydrogen H is almost negligible and this is because under the conditions of the temperature and the number density of each type of particle, the dissociation reaction rate is much larger than the recombination reaction rate. Therefore, when the particles are transported into the flow field, the number of molecular hydrogen $H_2$ decreases whilst the atomic hydrogen H increases. This affects the number density distribution for each type of particle.

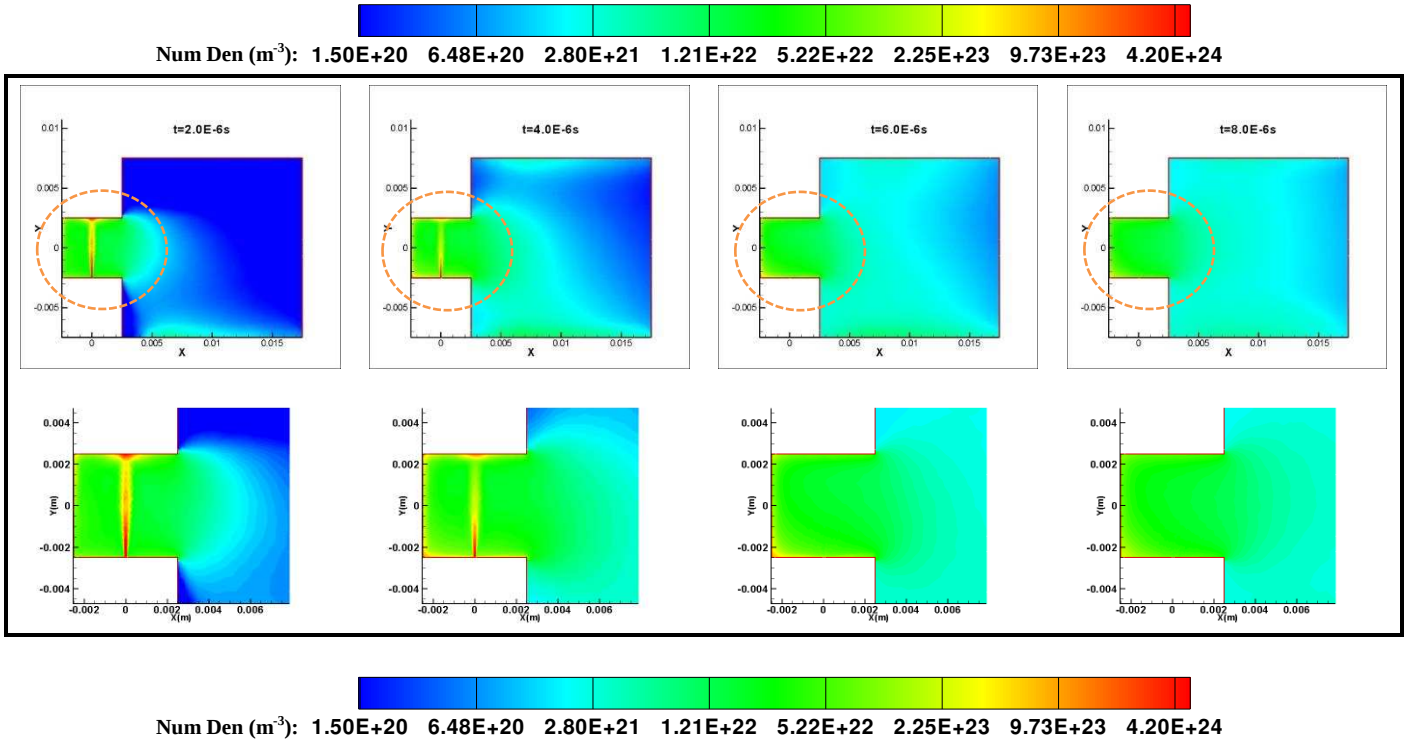

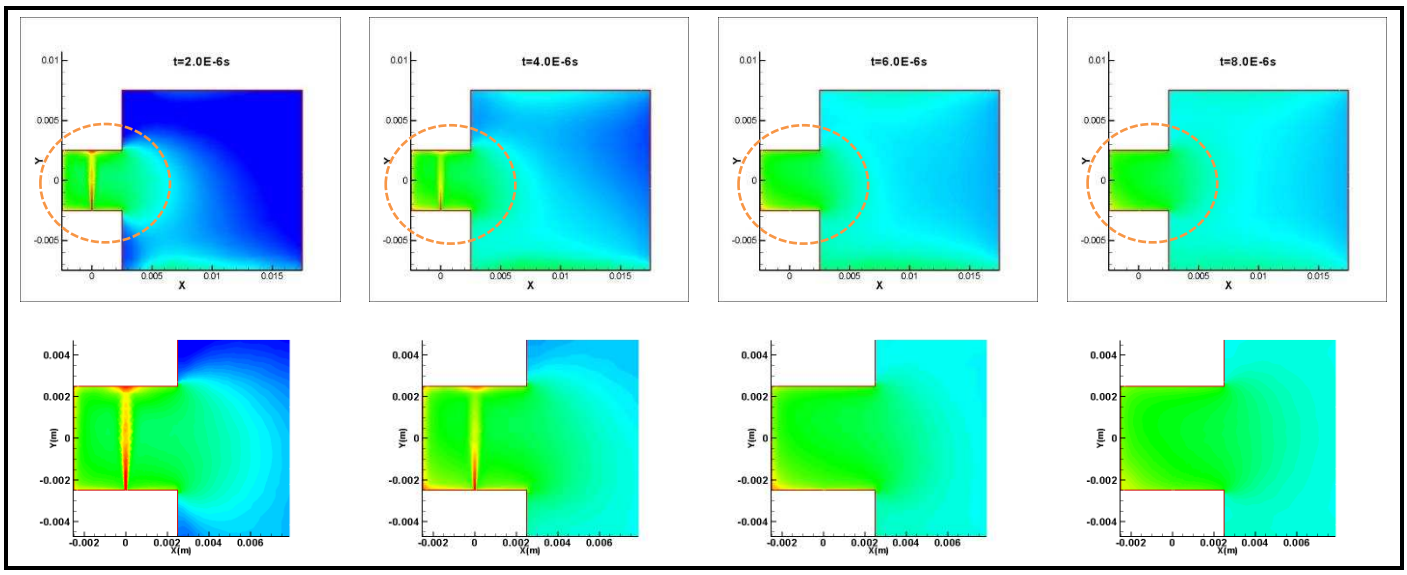


Fig. 9. The evolution of the number density of all the particles in the symmetric plane. The upper figure is the result without the chemical reaction models, and the lower figure is the result with the inclusion of the reaction models.

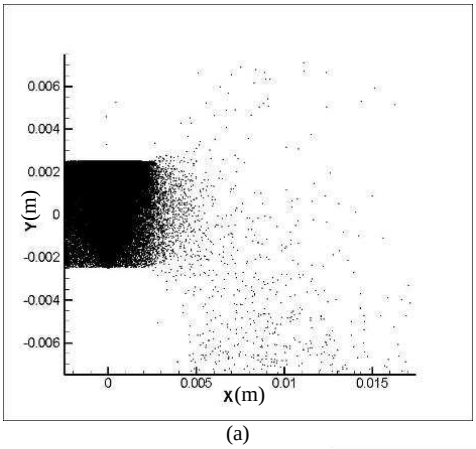


(a)

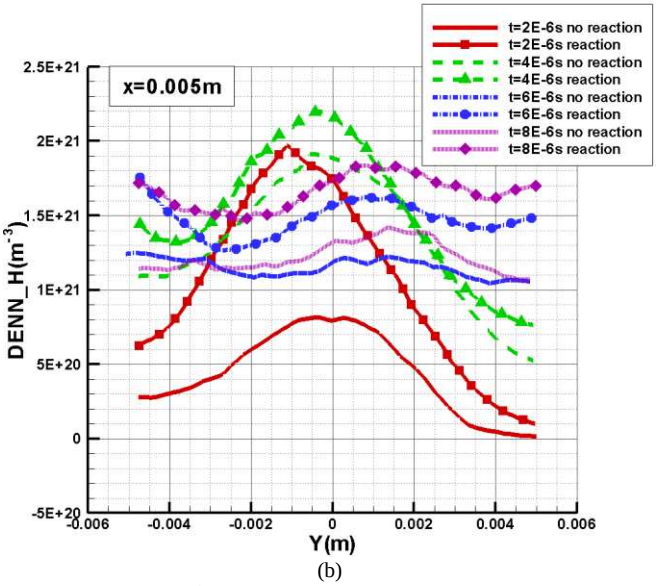


(b)

Fig. 10. The location of the molecular hydrogen $H_2$ where the dissociation reaction occurs in the flow field (a) and the number density of the atomic hydrogen H along the line with X = 0.005 m in the symmetrical plane (b).

Fig. 10 shows the location of the molecular hydrogen $H_2$ where the dissociation reactions occur and the number density distribution of the atomic hydrogen H along the line with X = 0.005 m in the symmetrical plane. Clearly, there are a large number of reactions for molecular hydrogen in the smaller cylinder. The relationship between the particle number density and the dissociation reaction can be observed to be such that the number density is high, as is the probability of the dissociation reaction. Due to the decomposition of $H_2$, the number density of the atomic hydrogen H is increased, and it is also different from that without the reactions.

Fig. 11 and Fig. 12 are, respectively, the molecular hydrogen $H_2$ and atomic hydrogen H number density contour in the symmetric plane without (upper) and with (lower) chemical reactions. As can be seen from Fig. 11, a majority of the molecules $H_2$ decompose in the smaller cylinder, and thus the number density of the molecules $H_2$ moving into the larger cylinder decreases. When the particle injection is stopped, the distribution of the molecules $H_2$ quickly becomes almost constant, even when the chemical reactions are not considered. As for the flow field with the chemical reactions, due to the decrease in the number of the molecules $H_2$, it is difficult for the molecules $H_2$ to become uniform in a short period of time, and the number density near the wall is much larger than that in the central region as shown in Fig. 11 (t = 6 - 8 μs).

As shown in Fig. 12, the atoms H pile up on the upper side of the larger cylinder at the time 2 μs. After that, the atoms H expand quickly into the whole field. Thus, due to the increase in the number of the atoms H from the chemical reactions, the expansion rates of H to make the flow uniform in the flow field are larger than those without reactions. Meanwhile, there are many atoms H accumulated near the wall of the small cylinder and this is because most of the $H_2$ dissociation reactions occur in this region.

The number density of the neutral particle X is not shown here because it does not take part in the chemical reactions and it has no impact on the distribution of the other particles no

matter whether or not the chemical reactions are considered. As shown in the distribution of these three types of particles, the particle number density varies with the chemical reactions considered or not. Under the chemical reaction conditions, the transportation of the total number of particles are faster because the amount of H increases and the weight of the atom H is small, and therefore it is easier to change the trend in their movement. After the particles stop being injected, the particle expansion decreases and this is because of the reduction in the number of $H_2$. It can be observed that the particle number density near the wall is larger than that in the central region near the axis, and the distribution of the overall particles is not homogeneous in the whole flow field.

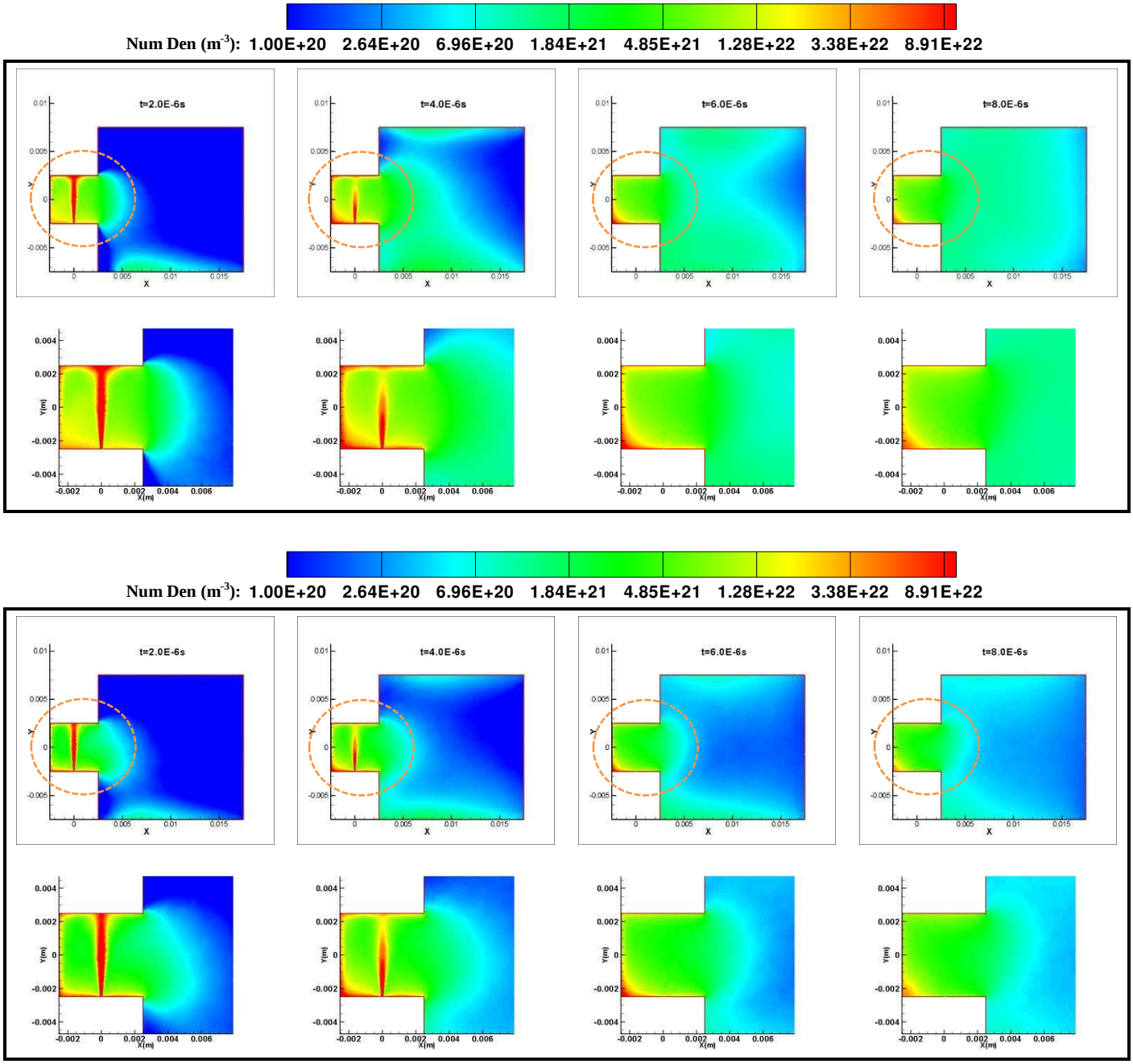


Fig. 11. The evolution of the number density of the molecular hydrogen $H_2$ in the symmetrical plane. The upper figure is the result without the chemical reaction models, and the lower figure is the result with the reaction models.

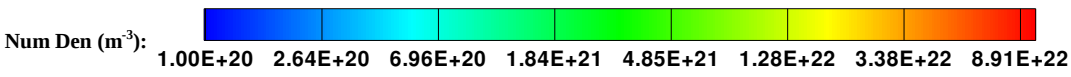

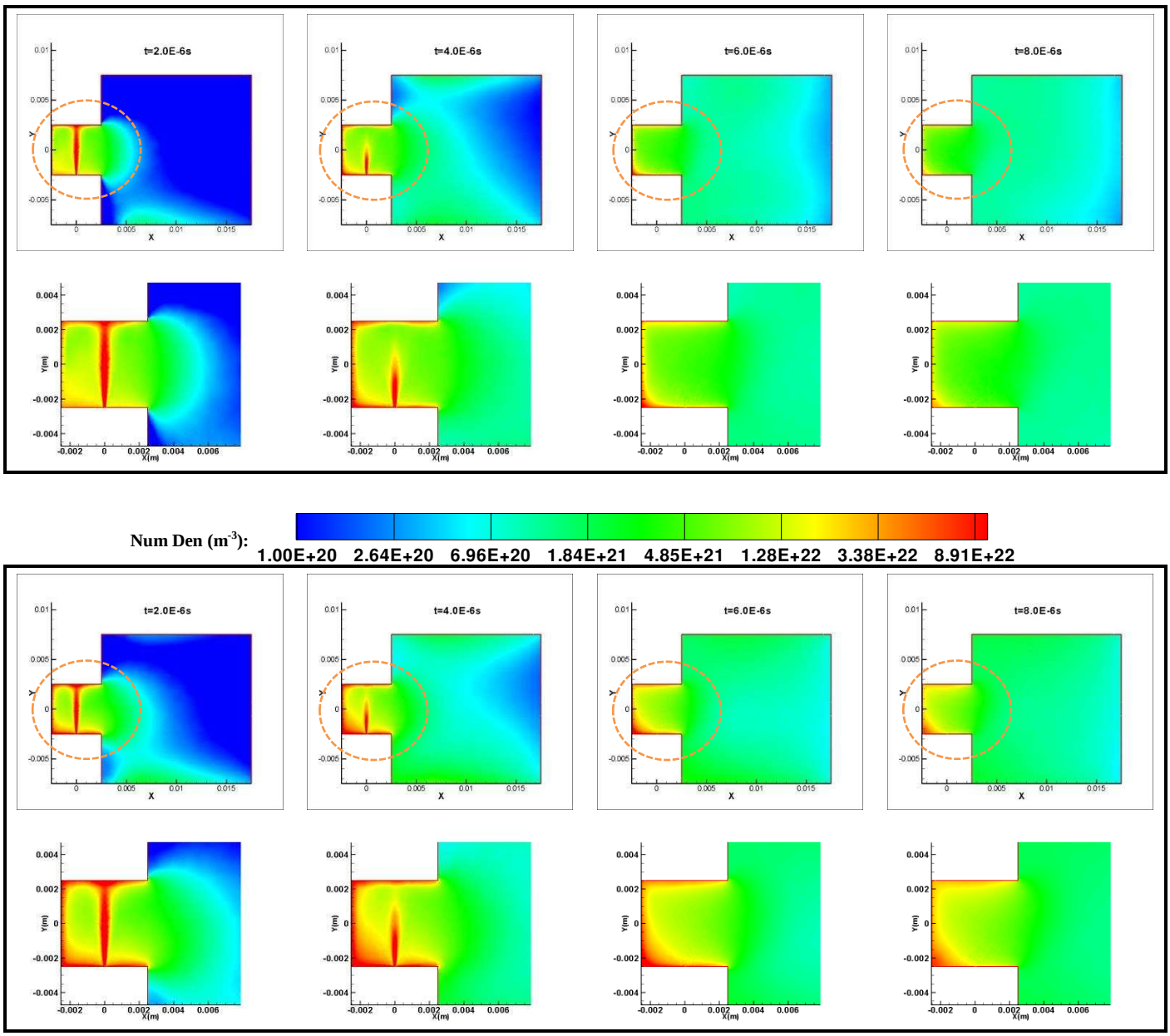


Fig. 12. The evolution of the number density of the atomic hydrogen H in the symmetrical plane. The upper figure is the result without the chemical reaction models, and the lower figure is the result with the reaction models.

## IV. Numerical Simulation of the Axisymmetric Plasma Flows with the Chemical Reactions Based on the DSMC / PIC Method

### A. Simulation Methods

For the DSMC and PIC methods, the requirements of the grid spatial scales are different. The DSMC method requires the grid spatial scale to be the magnitude of the molecular mean free path, while the PIC method requires it to be the magnitude of the Debye length. Therefore, there are two sets of grids in the numerical simulation, namely the unstructured grids for the DSMC method and the structured grids for the PIC method. Thus, the information between these two grids needs to be transmitted. The particles are moving and colliding in the unstructured grids, and therefore the information on the particles are stored based on the unstructured grids. However, the PIC method used to simulate the electric field is based on the structured grids, and the information on the particles in the structured grids needs to be known. Meanwhile, as for the movement of the ions, the accelerations of the ions are obtained by solving the distribution of the electric field, and the information of the electric field is stored based on the mesh nodes of the structured grids. Thus, firstly the force acting on the ions in the electric field should be calculated in the structured grid, and then interpolated into the unstructured grid in order to calculate the movement of the ions. Due to the regularity of the distribution of the structured grids, the mesh information of the particles in the structured grid can be obtained by the coordinates of the particles in the flow field.

As the plasma in the flow field is electrically neutral, therefore the Boltzmann relation for the electric potential field is obtained from the electron momentum equation using the

following assumptions: the electrons are isothermal and have constant temperature without any collisions, and the electron pressure obeys the ideal gas law, and the electrons are not magnetized [16]-[17]. Thus the Boltzmann relation can be given by [16]:

$$\Phi = \Phi_r + T_e \ln\left(\frac{n_e}{n_r}\right) \quad (4)$$

where $\Phi_r$ is the reference electric potential and $n_r$ is the reference electron number density. In addition, $T_e$ is the electron temperature in eV, and ne is the electron number density. In the simulations, the inlet is selected as the reference point, and the electron number density in each grid node is set to the ion number density based on the assumption of a quasi-neutral plasma. The electric potential of the reference point at the inlet is set to 0 Volts, so the values of the electric potential solved by the Boltzmann relation are negative. Since both the electric potential and the electron number density in (4) are based on the mesh nodes, the area weighting method [18]-[19] needs to be used so that the electric charges of the ions can be distributed to the mesh nodes. The variable hard sphere (VHS) model [9] is used for the collisions between neutral particles. There are two types of collisions between neutral particles and charged particles, one is the momentum exchange collision (MEX), the other is the charge exchange collision (CEX) [20]. Currently the study of these two types of collisions are focused on the species Xe, $Xe^+$, $Xe^{2+}$ in the Hall thrusters [17]. The data for the collisions of $H_2$, H, $H_2^+$, $H^+$ in the literature are very rare, thus the collisions are simplified here. The momentum exchange collision between the neutral particles and the charge particles is considered to be the variable hard sphere model as for the neutral particles, and the charge exchange collision is not considered here. Also there are many complicated chemical reactions in this flow field, such as the dissociation-recombination reactions and the ionization-neutralization reactions. In this simulation, the flow field is assumed to be weakly electric neutral, and the electrons are not individually simulated, they are represented by the simulated particles of the ions, so only the dissociation-recombination reactions for the neutral particles are considered.

## B. Simulation conditions

Fig. 13 shows the geometry of the computational domain with length 0.02 m and radius 0.01 m. The particles enter into the field from the inlet with the diameter 100 μm, as shown by the red line. The black lines represent the wall, the green lines indicate the free flow boundary and the brown lines are the symmetrical plane. The temperature of the wall is 300 K, and the diffusion reflection model is used for the gas-surface interactions. The charged particles which reach the wall will immediately be changed to be neutral particles. While ensuring that the plasma flow field is electrically neutral, it is assumed at the same time when the electrons reach the wall that they disappear, so the potential of the wall is considered to be zero. For the symmetric plane, the specular reflection model is used, and the radial electric potential is zero. The particles are composed of $H_2$, H, $H_2^+$ and $H^+$, and the speed of the neutral particles and charged particles are not the same. At the inlet, the temperature of the electrons is 5 eV, the temperature of the neutral particles is 3000 K and the velocity is 5000 m/s. The detailed inlet conditions are shown in Table II.

TABLE II
THE INLET CONDITIONS OF THE PARTICLES

| Species | Number Density ( $/m^3$ ) | Temperature ( K ) | Velocity ( m/s ) |
|---|---|---|---|
| $H_2$ | $3\times10^{24}$ | 3000 | 5000 |
| H | $1.5\times10^{24}$ | 3000 | 5000 |
| $H_2^+$ | $1\times10^{23}$ | 3000 | 5000 |
| $H^+$ | $4\times10^{23}$ | 0.5 ev | 10000 ( Case 1) |
| | | | 15000 ( Case 2) |
| | | | 20000 ( Case 3) |

Since the scales of the grids suitable for the DSMC and PIC methods are different, there are two sets of grids. One based on unstructured grids for the DSMC method, the other one based on the structured grids for the PIC method as shown Fig. 13. For both of these methods, local mesh refinements are used. In the simulation, 9218 nodes and 47395 tetrahedral volume elements are used for the DSMC method, and 3000 hexahedral volume elements are used for the PIC method. The time step is about $4\times10^{-10}$ s, and the solutions were averaged over 50000 iterations.

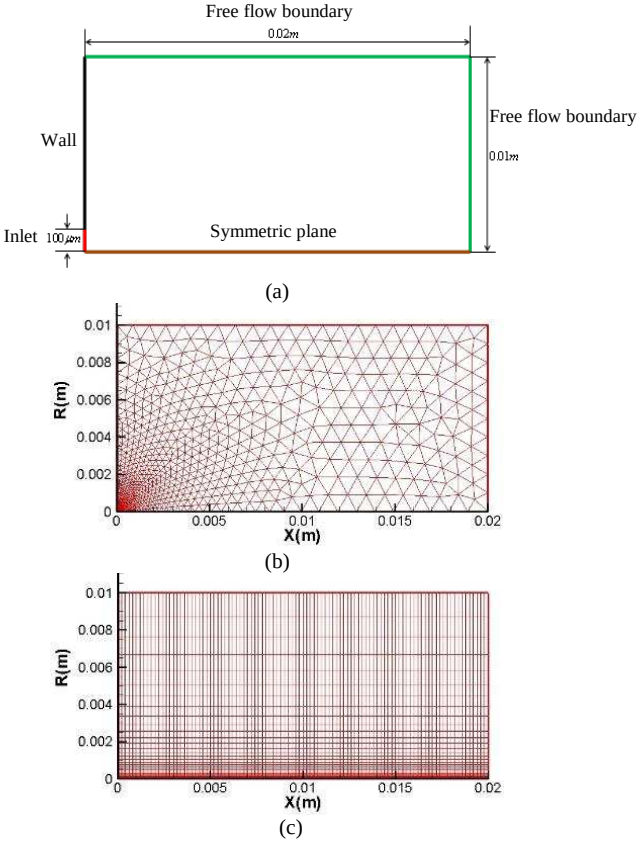


Fig. 13. The computational domain (a) and the grids (b) (c) employed in the simulations for the flow field and the electric field. The domain (a) is half of the cylinder with the radius being 0.01 m and the length being 0.02 m. The grids (b) are unstructured for the DSMC code, and the grids (c) are structured for the PIC code.

C. Results and discussion

Fig. 14 and Fig. 15 are the number density of the particles with and without the PIC modules. The upper ones are the distribution of the particle number density without the PIC model, and the lower ones with the PIC model. Fig.16 shows the number density along the axis, and it is observed that the particle number density decreases exponentially along the axis as well as in the radial directions. This decrease in the number density is the typical characteristics of the plume in a vacuum. The particles become very dilute after a certain distance away from the inlet, and therefore the physical parameters near the inlet are investigated here. On the whole, the particle number density decreases in all directions away from the inlet. Since the main flow direction is along the axis, the change in the number density along the axis is less than that along the other directions, and the gradient of the changes in the number density increases with the increase in the flow angle with the axis.

Without considering the electric potential field, the neutral particles disperse more widely when the inlet velocity of the charged particles increases. Even at the same location in the flow field, the inlet velocity of the charged particles is larger, and the neutral particle number density is smaller. This is because the charged particles move so quickly, and when the charged particles collide with the neutral particles, then part of the energy transfers to the neutral particles, thus the speed of the neutral particles can be increased. As the speed of the charged particles becomes higher, then clearly the speed of the neutral particles increases and the expansion range also increases. In contrast, due to the increase in the ion number when the inlet velocity increases, the inlet velocity of the charged particles increases, and as well as the particle number density.

Considering the electric potential field, as shown in Fig. 14 - Fig. 16 with the PIC model, when the inlet ion velocity increases, the number density of the neutral particles decreases and the number density of the charged particles increases. The distribution of the neutral particles follows the same behavior as that the number density gradient in the axial direction is smaller than that in other directions, whether or not the electric field is considered. However, for charged particles, the behavior is different. When the PIC module is calculated, i.e. the electric potential field is considered, the discrepancy in the gradients along each direction becomes smaller. Meanwhile, the number density with the PIC module is generally lower than that without considering the PIC module. This is because the self-consistent electric field will be generated during the process of the movement of the charged particles, which will cause the acceleration of the charged particles, so the speed of the charged particles is clearly increased. After the speed of the charged particles accelerate significantly in the electric field, the distribution range of the charged particles becomes large, which will cause the number density of the particles to be lower than that without the electric field. Although the electric potential field does not directly affect the neutral particles, the acceleration of the charged particles will transfer to the neutral particles through the collisions between the charged and neutral particles. Therefore the velocity of the neutral particles will increase and the distribution range is large. As for the charged particles, the number density of the neutral particles with the PIC module is lower than that without the PIC module, and the decrease in the number density of the charged particles is greater than that of the neutral particles.

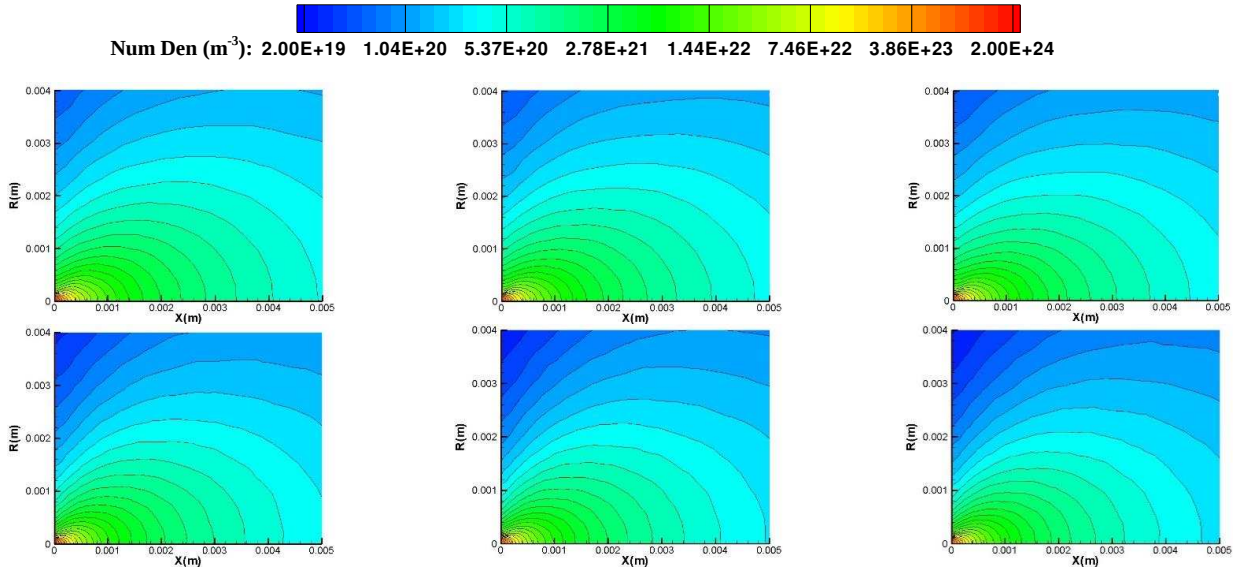


Fig. 14. The number density contours of the atom H in the flow field. The upper figure are the results obtained without the PIC model, the lower figure are those with the PIC model. On the left the results are obtained for the Case 1 with the inlet velocity of the ions 10000 m/s, the middle results are for the Case 2 with the inlet velocity of the ions 15000 m/s, the right results are for the Case 3 with the inlet velocity of the ions 20000 m/s.

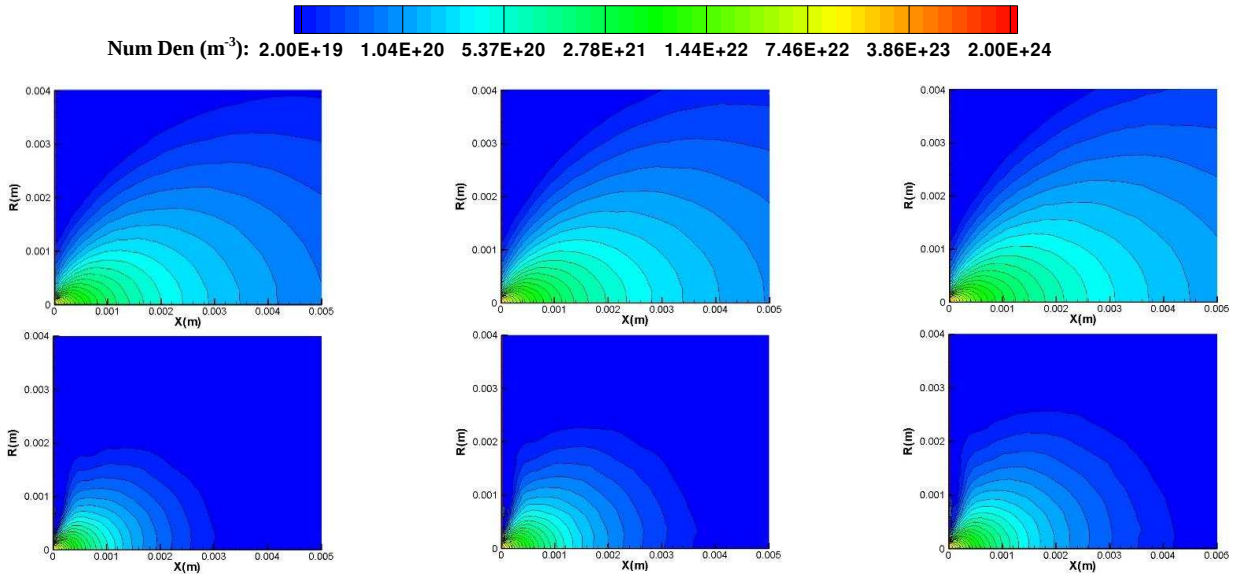


Fig. 15. The number density contour of the ion $H_2^+$ in the flow field. The upper figure are the results obtained without the PIC model, the lower figure are those with the PIC model. On the left the results are obtained for the Case 1 with the inlet velocity of the ions 10000 m/s, the middle results are for the Case 2 with the inlet velocity of the ions 15000 m/s, the right results are for the Case 3 with the inlet velocity of the ions 20000 m/s.

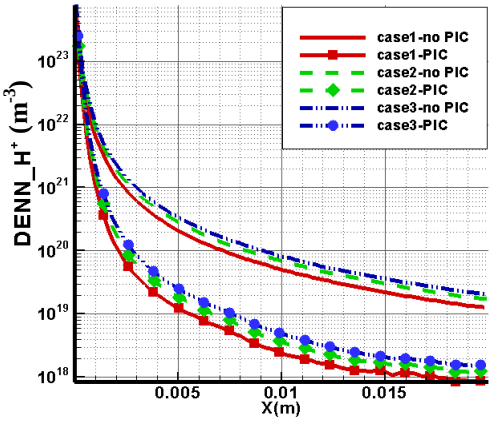


Fig. 16. The number density of the ion $H^+$ along the axis in the three cases both with and without the PIC model.

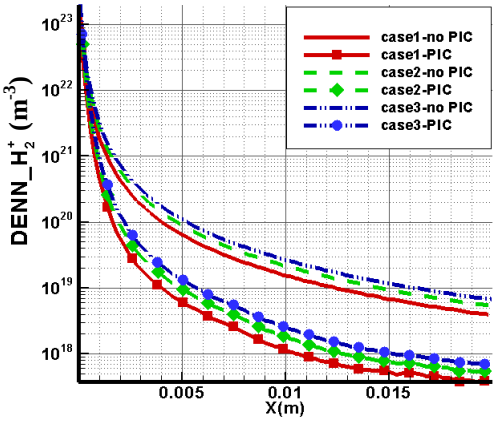


Fig. 17. The number density of the ion $H_2^+$ along the axis in the three cases both with and without the PIC model.

Fig.18 shows the distribution of the electric potential with the three different values of the ions velocity at the inlet. The potential distribution is related to the ion number density distribution, and the electric potential will be high where the number density is high. Since in all these cases the inlet is considered to be the zero potential reference plane and the ion number density in the flow field is generally less than that in the inlet, the electric potential in the flow field is negative. Comparatively, it can be observed that the potential distribution is similar to the ion number density distribution. In addition, the ions pile up near the inlet, so there is a large gradient in the electric potential near the inlet, and the potential changes away from the inlet are relatively not significant. The distribution of the electric field can be obtained by analyzing the potential distribution. As can be seen in Fig.18, the potential starts to decrease in all the directions away from the inlet. Thus, the electric field is radially distributed from the inlet in the flow field, and the electric field intensity decreases as the distance increases. Increasing the initial velocity of the ions from the inlet produces an increase in the ion number density, and this results in a simultaneous increase in the electric potential. This is because the electric potential is related to the electron number density according to the Boltzmann relation under the conditions of the same reference parameter for the potential and the electron number density.

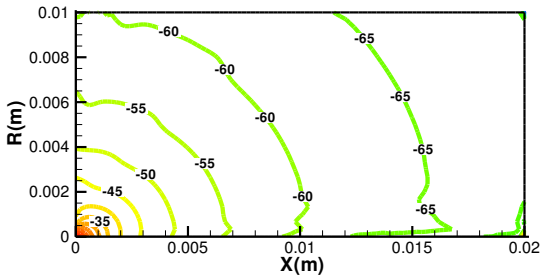


(a)

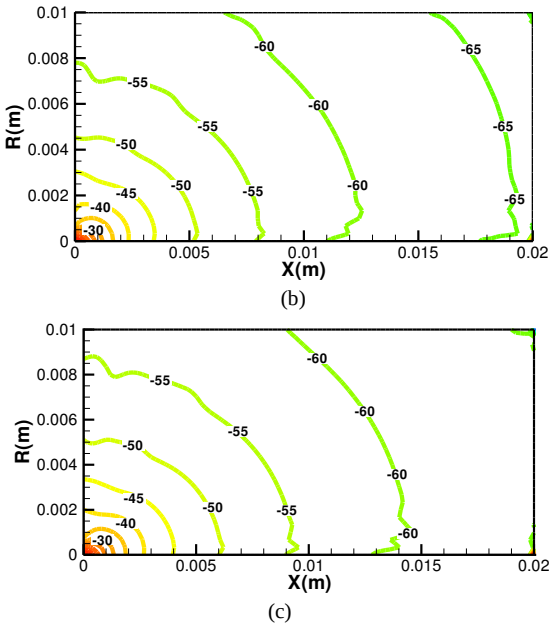


Fig. 18. The electric potential distribution with the three different values of the inlet velocity of the ions. The left result is for the Case 1 with the inlet velocity of the ions 10000 m/s, the middle result is for the Case 2 with the inlet velocity of the ions 15000 m/s, and the right result is for the Case 3 with the inlet velocity of the ions 20000 m/s.

## V. Conclusions

In the current study, the 3-D unsteady neutral particles chemically reactive rarefied flow has been investigated numerically using the in-house DSMC code which is compared with a case from the open literature in order to verify its accuracy. Under the simulation conditions, although the combination and dissociation reactions are considered in the flow field, most of the reactions are the dissociation reaction of the molecular hydrogen $H_2$. Due to this kind of reaction, the number density of the atomic hydrogen H increases while that of the molecular hydrogen $H_2$ decreases. The neutral particles chemical reactions will not only significantly affect the number density of each species but also the trajectory of the particles. Based on the DSMC/PIC method, the axisymmetric plasma flows with chemical reactions have been investigated. The distribution of the neutral particles and the charged particles, the electric potential distribution are analyzed under different initial conditions. The parameter distributions in the flow field are basically similar if only the initial velocity of the ions from the inlet are changed. The electric potential distribution is positively relevant to the ion number density and the initial velocity of the ions. The properties of the neutral particles obtained in this investigation can be of much assistance in the investigation of the unsteady rarefied plasma arc jet flow with chemical reactions.

## References


[1] Brandon D. Smith and Iain D. Boyd, "Hybrid-PIC modeling of a high-voltage, high-specific-impulse Hall thruster," in Proc. 49th AIAA/ASME/SAE/ASEE Joint Propuls. Conf., San Jose, CA, 2013.

[2] Burak Korkut, Zheng Li, and Deborah A Levin, "3-D simulation of ion thruster plumes using octree adaptive mesh refinement," IEEE Trans. on Plasma Sci., vol. 43, no. 5, pp. 1706-1721, 2015.

[3] Lubos Brieda, Taisen Zhuang, and Michael Keidar, "Towards near plume modeling of a micro cathode arc thruster," in Proc. 49th AIAA/ASME/SAE/ASEE Joint Propuls. Conf., San Jose, CA, 2013.

[4] M Mozetic, K Ostrikov, D N Ruzic, D Curreli, and U Cvelbar, "Recent advances in vacuum sciences and applications," J. of Phys. D: Appl. Phys., vol. 47, pp. 153001-1530024, 2014.

[5] Yuki Hirata, Takahisa Kato, and Junho Choi, "DLC coating on a trench-shaped target by bipolar PBII," Int. J. of Refractory Metals and Hard Materials, vol. 49, pp. 392-399, 2015.

[6] Francesco Taccogna, Pierpaolo Minelli, Domenico Bruno, Savino Longo, and Ralf Schneider, "Kinetic divertor modelling," J. Chem. Phys., vol. 398, pp. 27-32, 2012.

[7] Cristian Gleason-González, Stylianos Varoutis, Volker Hauer, and Christian Day, "Simulation of neutral gas flow in a tokamak divertor using the Direct Simulation Monte Carlo method," Fusion Eng. and Design, vol. 89, pp. 1042-1047, 2014.

[8] Jin Seok Kim, Min Young Hur, In Cheol Song, Ho-Jun Lee, and Hae June Lee, "Simulation of low-pressure capacitively coupled plasmas combining a parallelized particle-in-cell simulation and direct simulation of Monte Carlo," IEEE Trans. on Plasma Sci., vol. 42, no. 12, pp. 3819-3824, 2014.

[9] Bird G A, Molecular Gas Dynamics and the Direct Simulation of Gas Flows, Oxford: Clarendon Press, 1994.

[10] H. Timko, K. Matyash, R. Schneider, F. Djurabekova, K. Nordlund, A. Hansen, A. Descoeudres, J. Kovermann, A. Grudiev, W.Wuensch, S. Calatroni, and M. Taborelli, "A one-dimensional particle-in-cell model of plasma build-up in vacuum arcs," Contrib. Plasma Phys., vol. 51, no.1, pp. 5-21, 2011.

[11] M. M. Hopkins, J. J. Boerner1, C. H. Moore, E. V. Barnat, P. S. Crozier, S. G. Moore, M. T. Bettencourt, R. B. Campbell, L. C. Musson, and R. W. Hooper, "Challenges to simulating vacuum arc discharge," in Proc. 31st ICPIG, Granada, Spain, July 14-19, 2013.

[12] Vladimir V Serikov, Shinji Kawamoto, and Kenichi Nanbu, "Particle-in-cell plus direct simulation Monte Carlo (PIC-DSMC) approach for self-consistent plasma-gas simulations," IEEE Trans. Plasma Sci., vol. 27, no. 5, pp. 1389-1398, 1999.

[13] Chris H. Moore, Matthew M. Hopkinsa, Paul S. Crozierb, Jeremiah J. Boernera, Lawrence C. Mussonc, Russell W. Hooperd, Matthew T. Bettencourtb, "1D PIC-DSMC simulations of breakdown in microscale gaps," in Proc. 28th Int. Symposium on Rarefied Gas Dynamics, 2012, pp. 629-636.

[14] Satoshi Tsuno, Takeshi Nakahagi, Ryutaro Yamashiro, Atsushi Nezu, Haruaki Matsuura, and Hiroshi Akatsuka, "Numerical study on acceleration and deceleration mechanism of weakly ionized plasma flowing supersonically through open field line," IEEE Trans. Plasma Sci., vol. 42, no. 12, pp. 3732-3741, 2014.

[15] Naβ A and Steffens E, "Direct simulation of low-pressure supersonic gas expansions and its experimental verification," Nuclear Instruments and Methods in Phys. Research A, vol. 598, pp. 653-666, 2009.

[16] Paul N Giuliano, Iain D Boyd, "Analysis of a plasma test cell including non-neutrality and complex collision mechanisms," in Proc. 48th AIAA/ASME/SAE/ASEE Joint Propuls. Conf., Atlanta, Georgia, 2012, paper AIAA 2012-3736.

[17] Iain D Boyd and John T. Yim, "Modeling of the near field plume of a Hall thruster," J. of Appl. Phys., vol. 95, no. 94, pp. 575-4584, 2004.

[18] Gatsonis N A and Gagne M, "Electron Temperature effects on pulsed plasma thruster plume expansion," in Proc. 36th AIAA/ASME/SAE/ASEE Joint Propuls. Conf., Huntsville, Alabama, 2000, paper AIAA 2000-3428.

[19] Birdsall C K, Langdon A B, Plasma physics via computer simulation, New York: McGraw-Hill, 1985.

[20] Iain D Boyd, "Hybrid particle-continuum methods for nonequilibrium gas and plasma flows," in Proc. 27th Int. Symp. Rarefied Gas Dyn., 2010.



**Jie Li** received the Ph.D. degree in fluid dynamics from National University of Defense Technology, Changsha, China, 2004.

She is an Associate Professor with the college of Aerospace Science and Engineering, National University of Defense Technology, China. She is currently a visiting scholar with University of Sheffield. Her current research interests include the

direct simulation Monte Carlo method, nonequilibrium gas and plasma flows.

**Derek Ingham** is a Professor with the department of Mechanical Engineering, University of Sheffield, UK. He is on the editorial board of 12 international journals, has written 16 research books, over 900 research papers in referred journals and over 40 confidential industrial reports. He has received funding from over 70 different organizations.

He has research interests in heat and fluid flows, Carbon capture and storage, turbulence, and computational fluid dynamics.

**Lin Ma** received the Ph.D. degree in the University of Leeds. He is a Professor with the department of Mechanical Engineering, University of Sheffield, UK.

He has co-authored over 160 pear reviewed research papers in leading scientific research journals and conferences, including the publication of two books and two patents. His research is in the field of future clean and sustainable energy technology with a focus on multi-scale energy process computational and CFD modelling. He has been participating in a number of major clean fuel and renewable energy technology research projects sponsored by RCUK, TSB, EU, and industry.

He is a member of the Energy 2050 initiative.

**Mohamed Pourkashanian** is the Head of University Energy Research at the University of Sheffield and Director of the Pilot-scale Advanced Capture Technology (PACT) national facilities. He is a Professor of Energy Engineering and has completed numerous major research projects on clean energy technology and has received a substantial sum of grants from RCUK-EPSRC, EU, NATO, and industry. He has published over 446 refereed research papers and has co-authored books on coal combustion.

He is a member of EERA Implementation Plan 2013-2015 (contribution to CCS-EII Team, SET-PLAN), a member of Coordinating Group of UKCCSRC, an invited member of the All Party Parliamentary Renewable Transport Fuels Group, member of technical working group for the Department of Energy & Climate Change (CCS Roadmap UK2050) and Expert-Member in EU-GCC Clean Gas Energy Network.